# The variable ionized absorber in the Seyfert 2 Mrk 348

E. Marchese<sup>1\*</sup>, V. Braito<sup>1</sup>†, J. N Reeves<sup>2,3</sup>‡, R. Della Ceca<sup>4</sup>, A. Caccianiga<sup>4</sup>, A. Markowitz<sup>5,6,7</sup>, G. Risaliti <sup>8,9</sup>, P. Severgnini<sup>4</sup>, T.J. Turner<sup>3</sup>

- <sup>1</sup>INAF Osservatorio Astronomico di Brera, Via Bianchi 46 I-23807 Merate (LC), Italy
- <sup>2</sup>Astrophysics Group, School of Physical and Geographical Sciences, Keele University, Keele, Staffordshire, ST5 5BG, UK
- <sup>3</sup>Department of Physics, University of Maryland Baltimore County, 1000 Hilltop Circle, Baltimore, MD 21250, USA
- <sup>4</sup>INAF-Osservatorio Astronomico di Brera, via Brera 28, 20121 Milano, Italy
- <sup>5</sup>University of California, San Diego, Center for Astrophysics and Space Sciences, 9500 Gilman Dr., La Jolla, CA 92093-0424, USA
- <sup>6</sup> Karl Remeis Sternwarte, Sternwartstrasse 7, 96049 Bamberg, Germany
- <sup>7</sup> Alexander von Humboldt Fellow
- <sup>8</sup> Harvard Smithsonian Center for Astrophysics, 60 Garden Street, Cambridge, MA 02138, USA
- <sup>9</sup>INAF Osservatorio Astrofisico di Arcetri, Largo E. Fermi 5, 50125 Firenze, Italy

#### **ABSTRACT**

We present the results of the analysis of the X-ray spectrum of the Seyfert 2 Mrk 348, observed by Suzaku and XMM-Newton. The overall spectrum of Mrk 348 can be described by a primary power law continuum seen through three layers of absorption, of which one is neutral and two are ionised. Comparing Suzaku (2008) and XMM-Newton (2002) observations we find variability of the X-ray spectral curvature. We suggest that the variability can be explained through the change of column density of both the neutral and one of the ionised absorbers, together with a variation of the ionisation level of the same absorber. We thus confirm one of the main features presented in past works, where intrinsic column density variability up to  $\sim 10^{23}~{\rm cm}^{-2}$  was observed on time scales of months. We also find that the photon index of the underlying power law continuum ( $\Gamma \sim 1.8$ ) is in agreement with the previous observations of this Seyfert 2.

**Key words:** galaxies: active – galaxies: individual (Mrk 348) – X-rays: galaxies – galaxy Mrk 348

#### 1 INTRODUCTION

The extreme energetic phenomena occurring in the nuclei of active galaxies (Active Galactic Nuclei, AGN) are now recognized to be the result of accretion of large amounts of gas onto a central supermassive black hole (SMBH), which grows and emits radiation covering a wide range of energies.

In the Unified Model of AGN (Antonucci 1993) their different observed properties are explained through orientation effects between our line of sight to the nucleus and "circum-nuclear material". This circum-nuclear gas imprints features - low energy cutoffs, the Compton hump and emission and absorption lines - onto the primary X-ray emission. However, recent studies have shown that AGN are more complex than the simple picture of the Unified Model, where the absorbing matter is uniformly distributed in a toroidal geometry, and located at a pc scale distance from the central region (Antonucci 1993; Urry & Padovani 1995). In fact, this

representation does not fully explain the features observed in all AGN (Bianchi et al. 2012; Turner et al. 2009, 2012; Elvis 2012), this is the reason why the geometry, size and physical state of the circum-nuclear medium of AGN are still a matter of debate.

Indeed, recent X-ray observations of nearby and bright AGN showed the co-existence of multiple absorbing components, tracing gas covering a wide range of column densities ( $N_{\rm H}$ ) and ionisation states, all of them contributing in giving shape and complexity to the X-ray spectrum we observe (see Turner et al. 2009).

The variability observed in the X-ray spectra of few nearby AGN showed that this matter is highly structured with a range of ionisation states, densities, geometries and locations (Turner et al. 2009, Risaliti 2010) and, in particular, that a significant fraction of the absorbing medium must be clumpy.  $N_{\rm H}$  variations have been discovered on various time-scales, allowing to constrain the location and size of the obscuring clumpy material. There is an increasing number of obscured or type 2 AGN displaying variability in the X-ray absorbers: NGC 1365 (Risaliti et al. 2005, 2007, 2009; Maiolino et al. 2010), NGC 4388 (Elvis et al. 2004), NGC 7674 (Bianchi et al. 2005), NGC 4151 (Puccetti et al. 2007), NGC 7582 (Xue et al. 1998;

<sup>\*</sup> E-mail:elena.marchese@brera.inaf.it

<sup>†</sup> E-mail:valentina.braito@brera.inaf.it

<sup>‡</sup> E-mail:j.n.reeves@keele.ac.uk

# 2 E. Marchese et al.

Turner et al. 2000; Bianchi et al. 2009), UGC 4203 (Risaliti et al. 2010), Cen A (Rivers, Markowitz, & Rothschild 2011), NGC 454 (Marchese et al. 2012) and NGC 4507 (Braito et al. 2013). A few of these sources represent the most extremes cases, known as "changing-look" AGN, which show rather strong variability, from a Compton-thin state  $(N_{\rm H}=10^{23}{\rm cm}^{-2})$  to a Compton-thick state  $(N_{\rm H} > 10^{24} {\rm cm}^{-2})$ , on time-scales from a few days down to a few hours. The short time scale of some of these occultation events, when detectable, implies that the obscuring clouds are located in the inner region of the AGN, thus in proximity of the accretion disk or in the Broad Line Region. However, the majority of observations show variations on longer times scales (of the order of months or year), due either to observational limitations or to the intrinsic nature of the source. Moreover, it is not always straightforward to discern if the X-ray variability is due to a change in the column density of the absorber or to a variation in the primary emission of the X-ray source. Neverthless, it is now known that variability of the X-ray absorbers is a common propriety in type 2 AGN (Risaliti et al. 2002) and its analysis can give multiple information on the structure of the circumnuclear matter.

Mrk 348, as we will discuss below, does not belong to the class of changing-look AGN, since it was not observed in a state with  $N_{\rm H} > 10^{24} {\rm cm}^{-2}$ ; nevertheless the variability in the absorbing column density along the line of sight allows us to infer that the absorbing material is not homogeneous and stable, but that has to be clumpy. The data discussed here give us information about the geometry, structure and possible location of the absorbers.

Markarian 348 (NGC 262) is a Compton-thin Seyfert 2 galaxy at z=0.015 (Khachikian & Weedman 1974; de Vaucouleurs et al. 1991). The first X-ray observation of this source was performed by Ginga, and provided evidence of an absorbed  $(N_{\rm H} \sim 10^{23} {\rm cm}^{-2})$ X-ray source, with photon index  $\Gamma \sim 1.7$  (Warwick et al. 1989). In terms of the unification schemes for Seyfert galaxies, the identification of Mrk 348 as a Seyfert 2 was further confirmed in a work published by Miller & Goodrich (1990) showing that this source is characterised by a broad (FWHM  $\sim 7400 \text{ km s}^{-1}$ ) H $\alpha$ -line component in polarized light. Mrk 348 is a relatively strong radio emitter and was observed by the Very Large Array (VLA) and the Multi-Element-Radio-Linked-Interferometer-Network (MERLIN, Unger et al. 1984; Antón et al. 2002). It is characterised by a flat radio spectrum continuing well into the infrared, as well as a core-dominated radio structure and rapid radio variability (Neff & de Bruyn 1983). The complex radio properties of this source and the difficulties in determining its orientation with respect to the line of sight make its classification into a radio-quiet or radio loud source uncertain (Simpson et al. 1996).

Mrk 348 was observed with the *Rossi X-Ray Timing Explorer* (*RXTE*) mission in twelve observations during the period December 29, 1996 to July 12, 1997. Smith et al. (2001) analysed these spectra and described the resulting time–averaged 3–20 keV spectrum by a power-law continuum ( $\Gamma \sim 1.8$ ) absorbed by a column density of  $N_{\rm H} \sim 10^{23} {\rm cm}^{-2}$ , plus a Fe K $\alpha$  emission line with equivalent width  $EW \sim 100$  eV, plus a Compton reflection component. They found variations in the intrinsic column density occurring over periods of typically weeks to months, with the largest change ( $\Delta N_{\rm H} \sim 10^{23} {\rm cm}^{-2}$ ), taking place on a time-scale of  $\sim 70$  days. They also found X-ray continuum variations with the shortest observed timescale of  $\sim 1$  day. Smith et al. (2001) also found that the Fe K $\alpha$  line flux did not change significantly during the multiple observations, deducing that much of the

line emission is produced in a layer of material with a rather constant sky coverage and thickness, as viewed from the nucleus. They modelled the Compton reflection component using PEXRAV (Magdziarz & Zdziarski 1995), finding that the data were consistent with a reflection strength of  $R \sim 0.3 - 0.8$ . The 2-10 keV luminosity measured in these observations was, depending on the  $N_{\rm H}$  of each observation, in the range  $0.8-3.4\times10^{43}{\rm erg~s}^{-1}$  (for  $H_0 = 50$ ;  $q_0 = 0.5$ ), a factor 3 higher than that measured by Ginga. Smith et al. (2001) suggested that the absorber in Mrk 348 could consist of individual clouds; motions in and out of the line of sight could explain the observed variations in  $N_{\rm H}$ . Akylas et al. (2002) analyzed the same data as Smith et al. (2001) but with additional 25 RXTE observations taken in May-June 1996. This analysis confirmed the spectral variability already observed by Smith et al. (2001). Finally, a more recent work by Singh et al. (2011) on the X-ray spectral properties of a sample of Seyfert galaxies, analysed the 0.5-10 keV XMM-Newton EPIC-pn spectrum of Mrk 348 (2002). They suggested the presence of two absorbers intercepting the primary radiation, a fully covering absorber, with  $N_{\rm H}\sim 7\times 10^{22}{\rm cm}^{-2}$  and a partial covering component, with  $N_{\rm H}\sim 1\times 10^{23}{\rm cm}^{-2}$  and covering fraction of  $C_f\sim 0.84$ . They also found a narrow Fe K $\alpha$  line with  $EW \sim 34$  eV.

Here we present the results of a Suzaku observation (June 2008, net exposure  $\sim 76$  ks) and the comparison with XMM-Newton observation (July 2002, net exposure  $\sim 31$  ks for EPIC-pn). We show that the spectrum of Mrk 348 can be described by a primary power-law continuum intercepting multiple absorbing components, with different ionisation states. We found that the variability of the  $N_{\rm H}$  of these layers can explain the observed differences between the XMM-Newton and Suzaku.

The structure of the paper is the following: in Section 2 we describe Suzaku and XMM-Newton observations and data reduction; in Section 3 we focus on the modelling of the 0.6–70~keV Suzaku spectrum to understand the nature of the X-ray absorption and to evaluate the contribution of the reflection and Fe  $K\alpha$  emission line on the primary continuum. In Section 4 we compare our Suzaku best-fit model with the XMM-Newton spectrum and analyse the variations in some of the best-fit parameters, i.e.  $N_{\rm H}$  and the ionisation parameters. Discussion and conclusions follow in Sections 5 and 6. Throughout this paper, a cosmology with  $H_0 = 70~km~s^{-1}$  Mpc $^{-1}$ ,  $\Omega_{\Lambda}$ =0.73, and  $\Omega_{\rm m}$ =0.27 is adopted.

#### 2 OBSERVATIONS AND DATA REDUCTION

#### 2.1 Suzaku

Mrk 348 was observed by the Japanese X-ray satellite *Suzaku* (Mitsuda et al. 2007) on 28th June 2008 for a total exposure time of about 88 ks.

Suzaku carries on board four X-ray Imaging Spectrometers (XIS, Koyama et al. 2007), with X-ray CCDs at their focal plane, and a non-imaging hard X-ray detector (HXD-PIN, Takahashi et al. 2007). At the time of this observation only three of the XIS were working: one back-illuminated (BI) CCD (XIS1) and two front-illuminated (FI) CCDs (XIS0 and XIS3). All together the XIS and the HXD-PIN cover the 0.5–10 keV and 12–70 keV bands respectively. The spatial resolution of the XIS is  $\sim 2$  arcmin (HEW), while the field of view (FOV) of the HXD-PIN is 34 arcmin radius. Data from the XIS and HXD-PIN were processed using v2.1.6.14

of the *Suzaku* pipeline and applying the standard screening parameters<sup>1</sup>.

#### 2.1.1 The Suzaku XIS analysis

The XIS data were selected in  $3 \times 3$  and  $5 \times 5$  editmodes using only good events with grades 0, 2, 3, 4, 6 and filtering the hot and flickering pixels with the script sisclean. The XIS response (rmfs) and ancillary response (arfs) files were produced, using the latest calibration files available, with the ftools tasks xisrmfgen and xissimarfgen respectively. The net exposure times are 76 ks for each of the XIS. The XIS source spectra were extracted from a circular region of 2.9' centered on the source, and the background spectra were extracted from two circular regions with radius 2.3', offset from the source and the calibration sources. The spectra from the two FI CDDs (XIS 0 and XIS 3) were combined to create a single source spectrum (hereafter XIS-FI), while the BI (the XIS1) spectrum was kept separate and fitted simultaneously. The net 0.5-10 keV count rates are:  $(0.793 \pm 0.003)$  counts s<sup>-1</sup>,  $(0.829 \pm 0.003)$  counts s<sup>-1</sup>,  $(0.709 \pm 0.003)$  counts s<sup>-1</sup> for the XISO, XIS3 and XIS1 respectively. We considered data in the range 0.6-10 keV for the XIS-FI and in the range 0.6-9 keV for the XIS-BI (ignoring the band 1.6-1.9 keV, due to the presence of instrumental calibration uncertainties). The difference on the upper boundary for the XIS1 spectra is because this CCD is optimised for the soft X-ray band, with higher background at higher energies. The net XIS source spectra were binned at the Suzaku energy resolution and then grouped to a minimum of 20 counts per bin in order to use  $\chi^2$  statistics.

# 2.1.2 The Suzaku HXD-PIN analysis

For the HXD-PIN data reduction and analysis we followed the latest Suzaku data reduction guide (the ABC guide Version  $2^2$ ), and used the rev2 data, which include all 4 cluster units. The HXD-PIN instrument team provides the background (known as the "tuned" background) event file, which accounts for the instrumental "Non X-ray Background" (NXB; Kokubun et al. 2007). The systematic uncertainty of this "tuned" background model is  $\pm 1.3\%$  (at the  $1\sigma$  level for a net 20 ks exposure, Fukazawa et al. 2009).

We extracted the source and background spectra using the same common good time interval, and corrected the source spectrum for the detector dead time. The net exposure time after screening was 73 ks. We then simulated a spectrum for cosmic X-ray background counts (Boldt 1987; Gruber et al. 1999) and added it to the instrumental one. Mrk 348 was detected at a level of 36.8% above the background.

Fitting this spectrum with a power law we obtain a photon index  $\Gamma=1.50^{+0.09}_{-0.09}$  and  $F_{(14-70~{\rm keV})}\sim1.5\times10^{-10}{\rm erg~cm^{-2}~s^{-1}}.$  The extrapolation of this flux in the 14–195 keV band gives  $F_{(14-195~{\rm keV})}\sim3.4\times10^{-10}{\rm erg~cm^{-2}~s^{-1}}.$  This flux is higher than the <code>Swiff-BAT</code> flux, which is  $F_{(14-195~{\rm keV})}\sim1.6\times10^{-10}{\rm erg~cm^{-2}~s^{-1}}.$  We also note that <code>Swiff-BAT</code> observation provides a different photon index,  $\Gamma\sim1.9$ , probably due to the

wider energy range. If we fit simultaneously Suzaku HXD-PIN and Swift–BAT spectra, fixing the photon indexes to the same value, we find  $\Gamma \sim 1.8$ ; if we extrapolate the flux in the 14–195 keV band for Suzaku HXD observation we find  $F_{14-195\mathrm{keV}}^{HXD} \sim 2.3 \times 10^{-10}\mathrm{erg}~\mathrm{cm}^{-2}~\mathrm{s}^{-1}$ , while the flux measured during Swift–BAT observations is  $F_{(14-195~\mathrm{keV})}^{BAT} \sim 1.6 \times 10^{-10}\mathrm{erg}~\mathrm{cm}^{-2}~\mathrm{s}^{-1}$ . The variation could be explained by the fact that Swift–BAT spectrum is an average of the observations made during 58 months, while HXD observation provides a snapshot of the spectrum, when the flux was possibly higher, therefore it is not surprising to find intrinsic variations between them.

#### 2.2 XMM-Newton

XMM-Newton observed Mrk 348 on July 18, 2002 with a total duration of about 50 ks. The XMM-Newton observatory (Jansen et al. 2001) carries, among its onboard instruments, three 1500 cm<sup>2</sup> X-ray telescopes, each with EPIC (European Photon Imaging Cameras) imaging spectrometers at the focus. Two of the EPIC use MOS CCDs (Turner et al. 2001) and one uses a pn CCD (Strüder et al. 2001). These CCDs allow observations in the range  $\sim$ 0.5–10 keV.

During this observation the pn, MOS1, and MOS2 cameras had the medium filter applied and they were operating in Full Frame Window mode. The data have been processed using the Science Analysis Software (SAS ver. 6.5) and analysed using standard software packages (FTOOLS ver. 6.1). Event files have been filtered for high-background time intervals, and only events corresponding to patterns 0–12 (MOS1, MOS2) and to patterns 0–4 (pn) have been used. The net exposure times at the source position after data cleaning are  $\sim\!31.5$  ks (pn),  $\sim\!38.3$  ks (MOS1) and  $\sim\!38.2$  ks (MOS2). The net count rate in the 0.5–10 keV band is  $2.078\pm0.008$  counts s $^{-1}$  (pn), 0.647  $\pm$  0.004 counts s $^{-1}$  (MOS1) and 0.650±0.004 counts s $^{-1}$  (MOS2). The effect of pile-up for this source is negligible.

The results of the analysis of the XMM-Newton observation were already published in past works (Singh et al. 2011; Guainazzi et al. 2011), describing a best-fit model composed of a fully covering absorber ( $N_{\rm H} \sim 7 \times 10^{22} {\rm cm}^{-2}$ ), and a partial covering component with  $N_{\rm H} \sim 10.5 \times 10^{22} {\rm cm}^{-2}$  and covering fraction of  $C_f \sim 0.84$ . Therefore for this work we will only use the pn data (the MOS spectra are consistent with it), in order to compare it to the Suzaku spectra.

#### 3 SPECTRAL ANALYSIS

All the models were fitted to the data using standard software packages (XSPEC ver. 12.6.0, Arnaud 1996) and including Galactic absorption ( $N_{\rm H,Gal}=5.86\times10^{20}{\rm cm}^{-2}$ ; Kalberla et al. 2005). In the following, unless otherwise stated, fit parameters are quoted in the rest frame of the source at z=0.015 and errors are at the 90% confidence level for one interesting parameter ( $\Delta\chi^2=2.71$ ).

#### 3.1 Suzaku spectral analysis

For the analysis we fitted simultaneously the *Suzaku* spectra from the XIS-FI (0.6–10 keV), the XIS1(0.6–9 keV) and HXD-PIN (14–70 keV). We set the cross-normalization factor between the HXD and the XIS-FI spectra to 1.16 (allowing it to vary by  $\pm 5\%$ ), as recommended for XIS nominal observation processed after

 $<sup>^1\,</sup>$  The screening filters all events within the South Atlantic Anomaly (SAA) as well as with an Earth elevation angle (ELV)  $<5^{\circ}$  and Earth day-time elevation angles (DYE\_ELV) less than  $20^{\circ}$ . Furthermore also data within 256s of the SAA were excluded from the XIS and within 500s of the SAA for the HXD. Cut-off rigidity (COR) criteria of  $>8\,\mathrm{GV}$  for the HXD data and  $>6\,\mathrm{GV}$  for the XIS were used.

<sup>&</sup>lt;sup>2</sup> http://heasarc.gsfc.nasa.gov/docs/suzaku/analysis/abc/

### 4 E. Marchese et al.

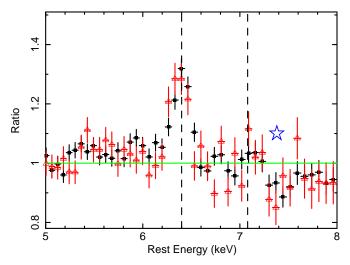


**Figure 1.** Data/model ratio between the *Suzaku* data (XIS-FI: black filled circles; XIS1: red open triangles, colours in the electronic version only) and a basic continuum model composed of an absorbed and an additional unabsorbed (scattered) power law, showing the iron line profile. The two vertical dashed lines correspond to the rest-frame energies of the Fe K $\alpha$  and Fe K $\beta$  emission lines at 6.4 keV and 7.06 keV respectively. The star indicates a possible absorption feature at  $\sim$  7.4 keV.

 $2008 \text{ July}^3$ . The cross normalization factor between the XIS-FI and the XIS1 spectra was allowed to vary.

As a starting point the data were fitted by a simple model composed of an absorbed primary power-law component and an unabsorbed power law, representing the fraction of primary X-ray radiation that is scattered into our line of sight. The photon indices of these two components were tied to each other. At this first stage we fitted only the continuum, excluding the data between 5 and 7.5 keV where we expected the Fe K $\alpha$  emission complex. This model provided a poor fit with a  $\chi^2$  of 411.4 for 266 degrees of freedom (d.o.f.), with a photon index  $\Gamma \sim 1.57$  and  $N_{\rm H} \sim 1.24 \times 10^{23} {\rm cm}^{-2}$ . When including the data in the 5–7.5 keV energy range we obtained  $\chi^2/d.o.f.=950/344$ . In Figure 1 we report the residuals of this simple model, including all data, which clearly reveal the presence of emission lines at energies corresponding to the Fe K $\alpha$  (E  $\sim 6.4$  keV), and Fe K $\beta$  (E  $\sim 7.06$  keV) emission lines.

We thus added two Gaussian components, in order to reproduce these emission lines, fixing the energy of the Fe K $\beta$  line to 7.06 keV and its normalization to be 13.5% of the Fe K $\alpha$  consistent with the theoretical value (Palmeri et al. 2003). The addition of the Fe K $\alpha$  and Fe K $\beta$  lines improved significantly the fit, yelding as energy centroid for the Fe K $\alpha$  line E=6.39 $^{+0.01}_{-0.01}$  keV and for the Fe K $\beta$  line E=7.10 $^{+0.06}_{-0.06}$  keV and a  $\Delta\chi^2=338.4$  for 3 d.o.f, with respect to the first model applied to all the data (including the 5–7.5 keV energy range). This was still not a good fit ( $\chi^2/d.o.f.=611.6/341$ ). The equivalent width of the Fe K $\alpha$  with respect to the observed continuum is  $EW=81.5^{+9.0}_{-8.8}$  eV, its energy centroid is  $E=6.39^{+0.01}_{-0.01}$  keV and  $\sigma=67.9^{+19.1}_{-21.0}$  eV. Considering that the Compton thin matter has an  $N_{\rm H}$  of  $\sim 1.2 \times 10^{23} \, {\rm cm}^{-2}$  we expect

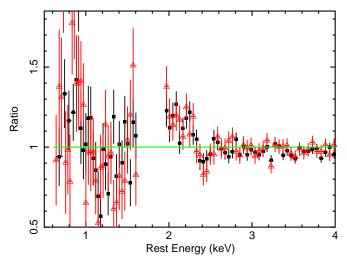


**Figure 2.** Data/model ratio in the soft X-ray energy region to the *Suzaku* data (XIS-FI: black filled circles; XIS1: red open triangles, colours in the electronic version only) and the model including the reflection component (modelled with PEXRAV). These residuals highlight the possible presence of an emission line at  $\sim 2.2$  keV and of an absorption line at  $\sim 2.4$  keV.

it to produce in transmission an equivalent width of  $EW\sim30~{\rm eV}$  for Solar abundances (Murphy & Yaqoob 2009). Therefore we can suppose that the measured Fe K $\alpha$  equivalent width is mainly due to reflection by Compton thick matter located out of the line of sight.

Given the presence of a flat continuum ( $\Gamma \sim 1.57$ ) and of the Fe K $\alpha$  emission with an equivalent width of  $EW \sim 81$  eV we included a Compton reflection component. This component was modelled by adding the PEXRAV model (Magdziarz & Zdziarski 1995). Fitting the model including this component we obtained  $\chi^2/d.o.f.=594.0/340$  (thus  $\Delta\chi^2=17.6$  compared to the model with the Fe K $\alpha$  and Fe K $\beta$  emission lines). The parameters characterizing the reflected component are: an inclination angle i fixed to  $60^\circ$ , abundance  $Z=Z_\odot$ , a reflection fraction (defined by the subtending solid angle of the reflector  $R=\Omega/4\pi$ ) found to be  $R\sim0.41$  and a normalisation fixed to the normalisation of the absorbed power law. The fact that the reflection is quite weak is in agreement with the modest equivalent width ( $EW\sim81$  eV) found for the Fe K $\alpha$  emission line (Ghisellini, Haardt, & Matt 1994; Matt, Brandt, & Fabian 1996).

The model still did not provide a good fit, in particular between 2 and 2.4 keV, as can be observed in Figure 2. Thus we added an emission line at about 2.2 keV and an absorption line at about 2.4 keV, even if we cannot exclude that these features could be instrumental features, such as the Au M edge. This provided a better representation of the soft X-ray spectrum, yielding a  $\chi^2$  of 534.1 for 336 d.o.f. ( $\Delta\chi^2$  of 59.9 for 4 d.o.f.). The energy centroids found for the lines are  $E=2.22^{+0.02}_{-0.02}$  keV and  $E=2.42^{+0.03}_{-0.03}$  keV. The model achieved until this point gives the following best-fit parameters:  $\Gamma=1.75^{+0.06}_{-0.05}$ ,  $R=0.41^{+0.17}_{-0.16}$ ,  $N_{\rm H}=1.29^{+0.28}_{-0.31}\times 10^{23}\,{\rm cm}^{-2}$ . Since there are still some residuals in the soft X-ray band we also added a thermal component, modelled through MEKAL (Mewe et al. 1985) in XSPEC.

<sup>3</sup> http://www.astro.isas.jaxa.jp/suzaku/doc/suzakumemo/suzakumemo-2007-11 pdf:

2007-11.pdf; We then replaced the neutral reflection component PEXRAV http://www.astro.isas.jaxa.jp/suzaku/doc/suzakumemo/suzakumemo-2008-06.pdf with the PEXMON model (Nandra et al. 2007) in XSPEC , which

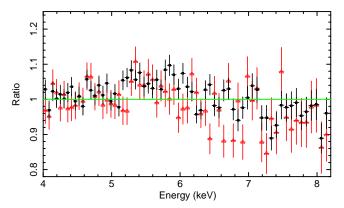


**Figure 3.** Data/model ratio in the 4–8 keV energy region between the *Suzaku* data (XIS-FI: black filled circles; XIS1: red open triangles, colours in the electronic version only) and the model including the reflection component (modelled with PEXMON).

self-consistently includes the Fe K $\alpha$ , Fe K $\beta$ , Ni K $\alpha$  and the Fe K $\alpha$  Compton shoulder. The parameters characterizing PEXMON are: an inclination angle i fixed to  $60^{\circ}$ , a cut off energy of E=200 keV (Dadina 2008), a scaling reflection factor R left free to vary, abundance  $Z=Z_{\odot}$ , and a reflection normalisation fixed to the normalisation of the absorbed power law. The fit including MEKAL and PEXMON gives a  $\chi^2/d.o.f.=514.3/337$ , and  $R=0.43^{+0.04}_{-0.04}$ . The fit is still poor due to the presence of residuals in the energy range 5–8 keV (see Fig. 3).

#### 3.1.1 Fe K complex

In this Section we discuss the possible presence of emission lines belonging to the Fe K complex and their properties. We looked for signatures of ionised emission lines, by adding a Gaussian component centered at  $E=6.7~{\rm keV}$  and then at  $E=6.96~{\rm keV}$ . The fit did not improve significantly and the upper limit on the equivalent width of each of these lines is less than  $10~{\rm eV}$ .

However, if we observe Figure 3, reporting the residuals of the last model, including the PEXMON component, the presence of a residual weak curvature between 5 and 6 keV and weak absorption lines near 7 keV is noticeable.

First we tested for the presence of broadening of the Fe K $\alpha$ emission line, due to relativistic effects manifesting when the line is produced in the inner regions of the accretion disk. Starting from the model including PEXMON, we added a Gaussian component initially centered at about E=6.4 keV, allowing its centroid energy to vary without any constraint. The addition of this component could account for the curvature only through a very broad and not so physical emission line centered at  $E \sim 5.6$  keV and with  $\sigma \sim 1$ keV. We finally attempted to add a component describing more precisely the line emission from a relativistic accretion disk. Thus we added the LAOR model in XSPEC (Laor 1991), representing the emission line profile from around a maximally rotating black hole. The outer radius  $R_{out}$  was fixed at 100  $R_q$ , the inclination was constrained to be  $>45^{\circ}$  (appropriate for a type 2 AGN) and we allowed as free parameters the emissivity index, the innermost radius  $R_{in}$  and the normalization. The fit still fails to reproduce the curvature, unless we allow to vary the inclination, reaching a best-fit value of 25° ( $\chi^2/d.o.f.=398.7/333$ ), but this produces more than one inconsistency. In fact it represents a face-on orientation (which is in disagreement with the classification of this source

as a Sy2 under classical Sy1/Sy2 unification schemes and the Fe K $\alpha$  line has an equivalent width of  $EW \sim 168$  eV which, without considering the narrow Fe K $\alpha$  emission line, would imply a reflection fraction of  $R \sim 1$ , in contrast with what we find  $(R \sim 0.4)$ . Given that it appears unlikely to originate from a disk line, we investigated (Section 3.1.2) if the curvature could be due to a more complex absorber.

#### 3.1.2 Ionized absorber

Since, as discussed in section 3.1.1 and shown in Figure 3, the presence of a weak residual curvature and of weak absorption features is clear, we evaluated if a more complex absorber (i.e. partial covering or ionised) was required by the present data.

Firstly, we included a partial covering absorber in the model, in addition to the fully covering one, resulting in a significant improvement of the fit, yielding  $\Delta\chi^2=111.9$  for 2 d.o.f.. The column density of this absorber is  $N_{\rm H}=1.20^{+5.11}_{-2.65}\times10^{23}{\rm cm}^{-2}$  and the covering fraction is  $f_{cov}=0.50^{+0.19}_{-0.14}$ . Despite this being a better fit we note that the curvature in the 5–6 keV region is still present. We then used the best-fit values obtained by (Singh et al. 2011), who adopted the same model, fixing the covering fraction to  $f_{cov}=0.84$  and finding  $N_{\rm H,part.cov.}=9.16^{+0.61}_{-0.67}\times10^{22}{\rm \,cm}^{-2}$  and  $N_{\rm H,ful.cov.}=6.79^{+0.33}_{-0.28}\times10^{22}{\rm \,cm}^{-2}$ . However the fit get worse by  $\Delta\chi^2=-11.2$  for 1 d.o.f.

We thus consider if this feature of the spectrum can be better described through an ionised absorber. We added a model representing a photoionized absorber, which is made using a multiplicative grid of absorption model generated with the XSTAR v 2.1 code (Kallman et al. 2004). This grid describes an ionized absorber parametrised by its turbolence velocity (here we used 5000 km s<sup>-1</sup>), its  $N_{\rm H}$  and its ionisation parameter, defined as:

$$\xi = \frac{L_{ion}}{nR^2} \tag{1}$$

where  $L_{\rm ion}$  is the ionising luminosity in erg/s between 1–1000 Rydbergs (13.6 eV to 13.6 keV), n is the hydrogen number density in cm $^{-3}$  and R is the radial distance in cm of the absorber from the ionising source. The outflow velocity is fixed to zero for simplicity. We obtained a significant improvement, providing a  $\chi^2/d.o.f.=385.6/335~(\Delta\chi^2=128.7~{\rm for}~2~{\rm d.o.f}$  with respect to the model described at the end of section 3.1); the parameters obtained with this fit are  $N_{\rm H}$  (neutral absorber) =  $5.85^{+0.61}_{-0.66} \times 10^{22}$  cm $^{-2}$ ,  $N_{\rm H}$  (ionized absorber) =  $1.49^{+0.10}_{-0.09} \times 10^{23}$  cm $^{-2}$  and a photoionization parameter of  $\log\xi=1.83^{+0.15}_{-0.14}{\rm erg}~{\rm cm}~{\rm s}^{-1}$ . The addition of this mildly ionised absorber succeeds in reproducing the curvature in the 5–6 keV energy range.

Despite being a better description of the data, this model still leaves some residual features in the region 6–7.5 keV, in particular an absorption feature at  $\sim 7.4$  keV.

As a first step we added an absorption line, modelled by an inverted Gaussian, with its centroid and width left free to vary. This yielded  $\Delta\chi^2=7.8$  for 3 d.o.f., with energy of the line  $E{=}7.40^{+0.07}_{-0.06}$  keV and  $\sigma\sim0.046$  keV, which implies a FWHM of  $\sim\!4400$  km/s. Despite this weak feature is not highly significant, the most likely candidate for it is blue-shifted ( $v\sim0.05c$ ) absorption due to the  $1{\rm s}{\to}2{\rm p}$  transition of H-like Fe (E=6.97 keV), while if we assumed a lower ionization state of Fe (i.e. Fe xxv) the corresponding blue-shift would be higher ( $v\sim0.1c$ ).

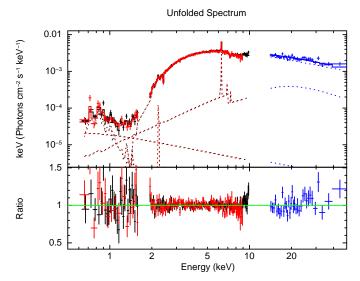


**Figure 4.** *Suzaku* 0.5–70 keV data and best-fit model (in the electronic version: XIS-FI black; XIS1 red; HXD blue) of Mrk 348; data have been rebinned for plotting purposes. The upper panel shows the data and best-fit model described at the end of section 3.1.2 (see table 2 for the best-fit parameters). The lower panel shows the data/model ratio to this model.

The last consideration lead us to investigate if the weak absorption feature could be well described by substituting the inverted Gaussian component with a second more ionized absorber. At this step, for simplicity, we tied the outflow velocity of the more ionised absorber to the velocity of the mildly ionised one, leaving it free to vary. The resulting fit with this additional component provided  $\chi^2/d.o.f.=369.3/332~(\Delta\chi^2=16.4~{\rm for}~3~{\rm d.o.f})$ , and gives an acceptable model for the absorption feature at  $\sim7.4~{\rm keV}$ . Then we tested for an improvement of the fit when leaving free to vary the outflow velocity of the highly ionised absorber. We obtained that the fit did not statistically improve  $(\chi^2/d.o.f.=364.6/331)$ . The same is true when we fixed the outflow velocity of the more ionised absorber to zero. Thus here-after we make the simple assumption that the two absorbers have the same outflow velocity. The model adopted is of the form

 $F(E) = \text{wabs} \times [\text{mekal} + (\text{zphabs} \times \text{ion abs}1 \times \text{ion abs}2 \times \text{pow}1) + \text{pexmon} + \text{pow}2 + 2.2 \text{keV emis.line} + 2.4 \text{keV abs.line})].$ 

The main parameters of the best fit model are:  $N_{\rm Hion1}=1.50^{+0.09}_{-0.09}\times10^{23}\,{\rm cm}^{-2},~N_{\rm Hneutral}=4.14^{+0.41}_{-0.40}\times10^{22}\,{\rm cm}^{-2},~N_{\rm Hion2}=1.41^{+0.80}_{-0.79}\times10^{23}\,{\rm cm}^{-2},\log\xi_1=1.63^{+0.08}_{-0.07}\,{\rm erg}\,{\rm cm}\,{\rm s}^{-1},\log\xi_2=3.88^{+0.09}_{-0.28}\,{\rm erg}\,{\rm cm}\,{\rm s}^{-1}$  and  $v_{\rm ion1,2}=0.057^{+0.006}_{-0.005}\,c$ . We note that, being the  $N_{\rm H}$  of the two ionised absorbers very similar, it could be due to a stratification of the same absorber with different ionisation states. This model for Suzaku gives a flux in the 2–10 keV energy range of  $F_{2-10{\rm keV}}\sim3.60\times10^{-11}\,{\rm erg}\,{\rm cm}^{-2}\,{\rm s}^{-1}$  and an intrinsic luminosity of  $L_{2-10{\rm keV}}\sim3.26\times10^{43}\,{\rm erg}\,{\rm s}^{-1}$ . The value of measured outflow velocity (0.057c) is in agreement with assuming an absorption feature due to blueshifted Fe XXVI absorption line.

Physically this model describes radiation that intercepts a neutral absorber and two photoionised absorbers that have an outflow velocity of  $\sim 0.06 {\rm c}$ , attenuating the primary AGN emission and producing blueshifted absorption lines.

# 4 XMM-Newton DATA ANALYSIS

Mrk 348 is candidate for a variable absorber (Akylas et al. 2002; Smith et al. 2001; Singh et al. 2011). The  $N_{\rm H}$  measured with Suzaku is a factor of 1.8 lower than the  $N_{\rm H}$  reported by Singh et al. (2011) from XMM-Newton in agreement with the presence of a variable absorber. Thus we re-analysed the XMM-Newton spectra with some of the models adopted for describing the Suzaku spectrum.

We first considered the simplest model, where the reflection is represented by PEXRAV plus a Gaussian component for the Fe K $\alpha$  emission line. When fitting simultaneously the Suzaku and XMM-Newton data we found that energy centroid of the Fe K $\alpha$  is consistent between the two observations, while its normalization changed (from  $I_{\rm Fe}^{Suzaku}=4.47^{+0.66}_{-0.65}\times 10^{-5}{\rm photons~cm^{-2}s^{-1}}$  and  $EW_{\rm Fe}^{Suzaku}=82^{+10}_{-10}$  eV to  $I_{\rm Fe}^{XMM}=2.37^{+0.63}_{-0.61}\times 10^{-5}{\rm photons~cm^{-2}s^{-1}}$  and  $EW_{\rm Fe}^{XMM}=47^{+13}_{-12}$  eV).

We then adopted the Suzaku best-fit model, where the presence of a reflector plus a Fe  $K\alpha$  and Fe  $K\beta$  emission lines was modelled by the PEXMON component. Given the observed variation of the Fe  $K\alpha$  emission line intensity we expect that, when applying the best-fit model simultaneously to Suzaku and XMM-Newton data, we need different reflection scaling factors of PEXMON.

In order to test the validity of this hypothesis, we investigated the following possible scenarios:

- (i) a variable continuum and a constant reflection component, i.e. a scenario in which the reflecting matter is quite far and does not respond immediately to the continuum variability. In terms of fitting parameters this is represented by
  - a free normalization of the primary power law between XMM-Newton and Suzaku;
  - the reflection parameters of XMM-Newton (reflection fraction R and normalization) tied to those of Suzaku.

The resulting fit yielded  $\chi^2 = 567.7$  for 407 d.o.f., and the assumption of constant reflection leaves residuals in the Fe K $\alpha$  region.

- (ii) a scenario where both the primary continuum and the reflection component were allowed to vary between *Suzaku* and XMM-*Newton* observations, i.e. a situation where a variability in the continum reverberates immediately in the reflecting material, which would be located closer in. Thus the fit was characterised by
  - a free normalization of the primary power law between XMM-Newton and Suzaku;
    - ullet a free reflection fraction  $R_{XMM}$  with respect to  $R_{Suzaku}$
  - The normalization of PEXMON tied to the normalization of the primary power law, for XMM-Newton and Suzaku independently

This representation lead to a better fit ( $\chi^2=551.1$  for 406 d.o.f.), where the continuum is unchanged (variations within the errors) while the reflection fraction does change, as expected.

Thus, we conclude that Suzaku and XMM-Newton observations do not show continuum variability, but the Fe K $\alpha$  emission line does show signs of variation between the two spectra. For this reason we consider hereafter that a good description is obtained by fixing between Suzaku and XMM-Newton the continuum and the PEXMON normalizations, while allowing the reflection fraction R free to vary between the two observations.

In Figure 5 we plot the Suzaku XIS (black, upper spectrum), HXD (blue) and XMM-Newton pn (red, lower spectrum) data (using the best-fit model, see below), confirming a change in the spectral curvature between 1 and 6 keV. We now analyse what are the spectral components that could be responsible for this variation. First of all we tested the model including the partial covering absorber. Fixing the covering fraction of both Suzaku and XMM-Newton to  $f_{cov}=0.84$  we obtain that the  $N_{\rm H}$  changes from  $N_{\rm H}_{part.cov}^{XMM}=1.55_{-0.13}^{+0.12}\times10^{23}{\rm cm}^{-2}$  to  $N_{\rm H}_{part.cov}^{Suzaku}=8.72_{-0.75}^{+0.69}\times10^{22}{\rm cm}^{-2}$  for the partial covering absorber, and from  $N_{\rm H}_{ful.cov}^{XMM}=1.16_{-0.05}^{+0.05}\times10^{23}{\rm cm}^{-2}$  to  $N_{\rm H}_{ful.cov}^{Suzaku}=6.93_{-0.31}^{+0.36}\times10^{22}{\rm cm}^{-2}$ . Now we consider as a starting

Now we consider as a starting point the best-fit model found for Suzaku, thus the model including the ionised absorbers. If we allow as free parameters only the  $N_{\rm H}$  of the neutral absorber together with the reflection R factor of PEXMON as well as the soft emission and absorption lines we found  $\chi^2/d.o.f.=589.8/409$ . The neutral absorber column density varies from  $N_{\rm H}^{Suzaku}_{\rm neutral}=4.27^{+0.50}_{-0.47}\times10^{22}{\rm cm}^{-2}$  to  $N_{\rm H}^{XMM}_{\rm neutral}=1.23^{+0.06}_{-0.06}\times10^{23}{\rm cm}^{-2}$ .

Since there are some residuals in the 6–8 keV region, we allowed as free parameters the column densities of the ionized absorbers. We obtained  $\chi^2/d.o.f.=568.7/407~(\Delta\chi^2=21.1~{\rm for}~2~{\rm d.o.f.})$ ; the parameters changing more significantly are the  $N_{\rm H}$  of the neutral absorber the  $N_{\rm H}$  of the mildly ionised absorber, implying that the source, when observed with XMM-Newton, is generally more absorbed than when observed with Suzaku.

We finally allowed also the ionization parameters to vary between Suzaku and XMM-Newton we obtained  $\chi^2/d.o.f. = 551.6/407$ . We found a similar variations for the  $N_{\rm H}$  of the different absorbers, as those mentioned above.

The ionisation parameter of the mildly ionised absorber change from  $\log \xi_1^{Suzaku} = 1.67^{+0.11}_{-0.10} {\rm erg~cm~s^{-1}}$  to  $\log \xi_1^{XMM} = 2.04^{+0.19}_{-0.18} {\rm erg~cm~s^{-1}}$ . This will be considered as the best–fit model and all the relative best-fit parameters are listed in table 2.

We note that if we untie the outflow velocity of XMM-Newton ionised absorbers with respect to Suzaku we find  $\Delta\chi^2=17$  with respect to the best fit model; the outflow velocity of the first ionised absorber is statistically unchanged, while for the second ionised absorber it is slightly lower ( $z=-0.020^{+0.006}_{-0.006}$ , corresponding to a velocity of 0.034c).

We remark that if we attempt to fix the  $N_{\rm H\,neutral}$  of XMM-Newton to the Suzaku best fit value, we get a worse fit by a factor  $\Delta\chi^2$ =20.

We conclude that we can account for the difference in the observed X-ray spectra between *Suzaku* and XMM-*Newton* through a variation in absorbing column density of both the neutral absorber and one of the ionised absorbers, together with a change in the ionisation parameter of the same ionised absorber.

We note that the measured values of  $N_{\rm H}$  found in this work are within the range of the column densities measured in past observations, in particular:

- $\bullet$   $\it Ginga$  (1987): the measured column density was  $\it N_{\rm H} \sim 10^{23} \rm \, cm^{-2}$
- ASCA (August 1996): as published by Awaki et al. (2000) the column density was  $N_{\rm H}\sim 1.6\times 10^{23}~{\rm cm}^{-2}$ . We note that during this observation the observed 2–10 keV flux was  $\sim 5\times 10^{-12}{\rm erg~cm}^{-2}~{\rm s}^{-1}$ , that is respectively a factor 5 and a factor 7 lower than what we observed with XMM-Newton and Suzaku. If we hypothesize a scenario where there is a delay in Fe K $\alpha$  response

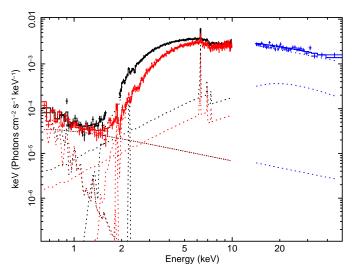


**Figure 5.** Comparison between the X-ray emission measured with *Suzaku* in 2008 (black data points in the electronic version) and XMM-*Newton* (red data points in the electronic version) in 2002. The continuum model is the best fit model composed of a primary power-law component transmitted trough a neutral absorber, a scattered power-law component, a Compton reflected component (modelled with PEXMON), and two ionized absorbers.

with respect to continum variations, this intrinsic variability in the continuum could be responsible for the different Fe  $K\alpha$  intensities discussed at the beginning of Section 4. In fact, the lower intensity Fe  $K\alpha$  line observed with XMM-Newton could be responding with a time delay to a different past continum (in this case a weaker continum) in a scenario where the reflector producing this emission line is far from the central variable X-ray source.

• *RXTE* (from mid 1996 to mid 1997, and in 2011):  $N_{\rm H}$  took values in the range  $0.9 - 3.2 \times 10^{23} \, {\rm cm}^{-2}$  during 14 months between mid 1996 and mid 1997 (Akylas et al. 2002; Smith et al. 2001) and in the range  $14 - 17 \times 10^{22} \, {\rm cm}^{-2}$  during the observation in 2011 (Markowitz, Krumpe, & Nikutta 2013)

We report for clarity in Figure 6 the measured values of  $N_{\rm H}$  of previous observations together with XMM-Newton and Suzaku observations.

#### 5 DISCUSSION

The presence of one or more ionized absorbers is not exceptional, indeed recent sensitive observations with *Chandra*, XMM-*Newton*, and *Suzaku* unveiled the presence of red- and blue-shifted photoionized absorption lines both in type 1 and type 2 AGN as well as in Radio Quiet and Radio Loud AGN (Tombesi et al. 2010, 2011, 2013; Gofford et al. 2013). Thus, it appears that there is a substantial amount of ionized gas in the nuclei of AGNs, which may be linked to gas outflowing on parsec scales with velocities from hundreds of km/s up to  $v_{\rm out} \sim 0.04-0.15c$  (Tombesi et al. 2010, 2012).

It is interesting to make a first order estimate of the maximum distance of this ionised absorber from the central black hole by means of the equation

$$R_{ion} = \frac{L_{ion}\Delta R}{N_{\rm H}\xi R} \tag{2}$$

Table 1. Summary of the X-ray emission lines detected for Suzaku spectrum in the 2–8 keV energy range. The energies of the lines are quoted in the rest frame. Fluxes and identifications are reported in column 2 and 3. The EW are reported in column 4 and they are calculated against the total observed continuum at their respective energies. In column 5 the improvement of fit is shown with respect to the continuum model, the value for the model with no lines is  $\chi^2/d.o.f.$ 

Energy	Flux	ID	EW	$\Delta \chi^2$
(keV)	$(10^{-6} \mathrm{ph} \ \mathrm{cm}^{-2} \ \mathrm{s}^{-1})$		(eV)	
(1)	(2)	(3)	(4)	(5)
$2.22_{-0.02}^{+0.02}$	$8.2^{+1.9}_{-1.9}$	$SK\alpha$		54
$2.42^{+0.03}_{-0.03}$	$-4.6^{+2.4}_{-2.5}$	Sxv		22
$6.39_{-0.01}^{+0.01}$	$44.8^{+5.0}_{-4.9}$	Fe K $\alpha$	$81.5^{+9}_{-8.8}$	335
7.06	13.5% Fe K $\alpha$	Fe K $\beta$		5
6.7	<4.8	Fe xxv	<12	0
6.97	< 5.8	Fe XXVI	<10	0

Table 2. Summary of the Suzaku and XMM-Newton parameters for the best-fit models described in section 3.1.2, and 4.

Model Component	Parameter	Suzaku	XMM-Newton	
		2008-06	2002-07	
Power law	Γ	$1.72_{-0.02}^{+0.02}$ $1.60_{-0.08}^{-0.08} \times 10^{-2}$ $2.66_{-0.41}^{+0.41} \times 10^{-5}$	fixed to $\Gamma_{Suzaku}$	
	Normalisation <sup>a</sup>	$1.60^{-0.08}_{-0.08} \times 10^{-2}$	fixed to norm <sub>Suzaku</sub>	
Scattered Component	Normalisation <sup>a</sup>	$3.66_{-0.42}^{+0.08} \times 10^{-5}$	fixed to norm <sub>Suzaku</sub>	
MEKAL	Normalisation <sup>a</sup>	$4.34^{+0.71}_{-0.70} \times 10^{-5}$	fixed to norm <sub>Suzaku</sub>	
	$k_{\mathrm{B}}T$	$0.24^{+0.02}_{-0.02}$	fixed to $kT_{Suzaku}$	
Neutral Absorber	$ m N_{H}$	$4.50^{+0.56}_{-0.51} \times 10^{22} \mathrm{cm}^{-2}$	$9.99^{-1.39}_{+1.32} \times 10^{22} \mathrm{cm}^{-2}$	
Reflection	R	$0.29^{+0.04}_{-0.04}$	$0.12^{+0.05}_{-0.05}$	
Ionised Absorber 1	$N_{ m H}$	$1.44^{+0.10}_{-0.10} \times 10^{23} \text{cm}^{-2}$	$2.11^{+0.19}_{-0.18} \times 10^{23} \text{cm}^{-2}$	
	$\log \xi$	$1.67^{+0.11}_{-0.10}$ erg cm s <sup>-1</sup>	$2.04^{+0.03}_{-0.01}$ erg cm s <sup>-1</sup>	
	z	fixed to z of Ionised Absorber 1	fixed to z of Ionised Absorber 1	
	$v_{turb}$	$5000 \ {\rm km \ s^{-1}}$	$5000 \ {\rm km \ s^{-1}}$	
Ionised Absorber 2	$N_{ m H}$	$1.31^{+1.22}_{-0.88} \times 10^{23} \text{cm}^{-2}$	$9.94^{+29.6}_{-0.57} \times 10^{22} \text{cm}^{-2}$	
	$\log \xi$	$3.87^{+0.11}_{-0.39}$ erg cm s <sup>-1</sup>	$3.73_{-0.27}^{+0.52}$ erg cm s <sup>-1</sup>	
	z	$-0.044^{+0.007}_{-0.006}$	fixed to $z_{Suzaku}$	
	$v_{ m turb}$	$5000 \text{ km s}^{-1}$	$5000  {\rm km  s^{-1}}$	
	$F_{(0.5-2)keV}$	$\sim 3.3 \times 10^{-13} {\rm erg \ cm^{-2} \ s^{-1}}$	$\sim 3.4 \times 10^{-13} {\rm erg \ cm^{-2} \ s^{-1}}$	
	$F_{(2-10)keV}$	$\sim 3.6  imes 10^{-11} { m erg \ cm^{-2} \ s^{-1}}$	$\sim 4.2 \times 10^{-11} { m erg \ cm^{-2} \ s^{-1}}$	
	$F_{(14-150)keV}$	$\sim 7.6 \times 10^{-12} {\rm erg \ cm^{-2} \ s^{-1}}$	$\sim 7.04 \times 10^{-12} {\rm erg \ cm^{-2} \ s^{-1}}$	
	$L_{(0.5-2)\mathrm{keV}}$	$\sim 1.72 \times 10^{43} {\rm erg \ s^{-1}}$	$\sim 1.73 \times 10^{43} {\rm erg \ s^{-1}}$	
	$L_{(2-10)keV}$	$\sim 3.26 \times 10^{43} {\rm erg \ s^{-1}}$	$\sim 3.17 \times 10^{43} { m erg \ s^{-1}}$	
	$L_{(14-150)keV}$	$\sim 4.51 \times 10^{42} {\rm erg \ s^{-1}}$	$\sim 4.20 \times 10^{42} { m erg \ s^{-1}}$	

<sup>&</sup>lt;sup>a</sup> units of photons keV $^{-1}$  cm $^{-2}$  s $^{-1}$ .

relating the ionisation parameter, the density of the absorber and the continuum luminosity  $L_{\mathrm{ion}}$ . In this case the estimate of  $L_{\mathrm{ion}}$ (in the energy range between 13.6 eV and 13.6 keV) from the best fit model is of the order of  $L_{\rm ion} \sim 7 \times 10^{43} {\rm erg \ s^{-1}}$ . Assuming that the thickness of the absorber,  $\Delta R = N_{\rm H}/n$ , is smaller than the distance  $R_{ion}$  ( $\Delta R/R_{ion} < 1$ ), we can set an upper limit to the distances of each ionised absorber, using Suzaku observations:

$$R_{ion} < \frac{L_{\rm ion}}{N_{\rm H}\xi}$$
 (3)

These upper limits are 0.026 pc and 2.72 pc for the highly and the mildly ionised absorber respectively. Despite being upper limits, they suggest that the likely location of these absorbers does not corresponds to the same radius with respect to the central source. The distance of the first ionised absorber is consistent in being a wind launched from a region located within the Broad Line Region.

The higher distance inferred for the mildly ionised absorber is due to the lower ionisation parameter, with respect to the higly ionised absorber. Its location could correspond to the region of the molecular torus, at a parsec-scale distance from the central source. However as this is an upper limit, we should not exclude the possibility that we are observing across this wind, thus we are not viewing directly the inner radius, which could be located at sub-parsec scales. Another method to put a constraint on the possible location of these absorbers is to estimate a lower limit on the radial distance by determining the escape radius at which the material will be able to leave the system. This can be determined once we have an estimate

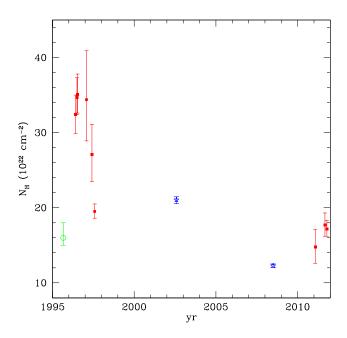


**Figure 6.** Comparison of the measured values of  $N_{\rm H}$  in ASCA observation (Awaki et al. 2000,green empty circles), in RXTE observation (red squares) during the time lag from 1997 to 2011 (Akylas et al. 2002 and A. Markowitz in prep. for the 2011 data) and the  $N_{\rm H}$  measured from Suzaku and XMM-Newton observations (blue stars, this work). The  $N_{\rm H}$  values of this work and of RXTE observations are based on the abundances relative to Solar reported in Wilms, Allen, & McCray (2000).

of the outflow velocity. Assuming spherical geometry, this radius is:

$$R_{esc} \geqslant \frac{2GM}{v_{out}^2} \simeq \frac{2c^2 R_g}{v_{out}^2}$$
 (4)

where  $R_g$  is the gravitational radius ( $R_g=GM/c^2$ ). Since the measured outflow velocity is  $\sim 0.055$  c, we obtain that  $R_{esc} \ge 660R_q$ . From the literature we have estimates of the mass of the central black hole, ranging from  $M_{BH} \sim 1.6 \times 10^7 M_{\odot}$  (Woo & Urry 2002) to  $M_{BH} \sim 7.5 \times 10^7 M_{\odot}$  (Nikolajuk, Papadakis, & Czerny 2004), so we can infer that  $R_g \sim 2.5 - 11.1 \times 10^{12} \mathrm{cm}$ , thus  $R_{esc} \geqslant 1.6 - 7.3 \times 10^{15} \text{cm} \sim 0.0005 - 0.002 \text{ pc}$ . This means that the wind may have been launched at least from a distance of the order of  $10^{-4} - 10^{-3}$  pc from the central black hole in order for it to escape, so an origin in the accretion disk or the Broad Line Region is plausible. In particular, this estimate suggests that the range of location of the first highly ionised absorber is between  $5 \times 10^{-4}$  pc and 0.026 pc in the Suzaku observation. However, another possibility could be that the wind is part of some aborted outflow, i.e. a wind with outflow velocity lower than the escape velocity and thus unable to leave the system; in that case we would only have an estimate of the maximum distance of the ionised absorber but not the minimum distance from which it was launched.

This analysis highlights the complexity and possible stratifications of the absorbers intercepting our line of sight. Indeed the observed spectrum could be explained with physically different scenarios: a unique and multi-phase absorber, where higher density (and lower ionisation) clouds are confined by lower density (higher ionisation) clouds, implying that the location of the two absorbers

are actually the same; or a configuration where there are effectively two winds at different physical states and distances, intercepting the line of sight. Neither of these two explanations can be ruled out at the moment, since higher spectral resolution observations are needed.

We conclude that the comparison between *Suzaku* and XMM-*Newton* observations of Mrk 348 does not show extreme variability, such as the transition from a Compton-thick to a Compton-thin state characterizing "changing look" AGN. However we cannot exclude that, given the long time elapsed between observations, we were not able to observe the source during an obscured Compton-thick phase. We do not observe a variation of the primary continuum, despite past RXTE observations which showed brightness variations on time scales down to 1 day (Smith et al. 2001). The satellite ASCA also observed the source (13 years earlier) in a state with flux 7 times lower than the flux observed with *Suzaku*.

Mrk 348 can be placed among the large number of AGN where a non uniform distribution of the circumnuclear absorbing matter determines  $N_{\rm H}$  variations in different epochs. This is consistent with recent theoretical models (Nenkova et al. 2008a,b) and works (Elitzur 2008, 2012) that indicate the possible clumpy nature of the torus, suggesting that the unified model of AGN is a too simplified scheme. The unified scheme is based on the assumption of a uniform torus, with the same opening angle for all AGN, implying that the viewing angle is the unique factor determining the classification into Type 1 and Type 2 AGN. This is clearly in conflict with both the  $N_{\rm H}$  variability and infrared observations (Lutz et al. 2004; Horst et al. 2006) showing that there is no significant difference in the mid-IR emission, normalized to the X-ray flux, of Type 1 and Type 2 AGN, contrary to the expectation of strong anisotropy of the unified model. As suggested by Elitzur (2012) these observations are compatible with a "soft-edged" clumpy torus.

#### 6 CONCLUSIONS

We presented the analysis of the X-ray spectrum of Mrk 348 obtained by *Suzaku* and compared it to the spectrum observed by XMM-*Newton*.

- $\bullet$  The best-fit model representing the observed X-ray emission is composed of a primary continuum intercepting three absorbers with different densities and ionisations (including one neutral absorber). We suggest that the location of the neutral absorber and of the mildly ionised absorber are at a parsec scale distance, thus consistent with the location of the putative torus. Instead, the highly ionised absorber appears to be located within  $\sim 0.03$  pc from the central source, likely in the Broad Line Region.
- The comparison with the XMM-Newton observation leads to the conclusions that: 1) the normalization and photon index of the primary and scattered power law do not vary between the two observations, despite such variations were observed in past observations (Smith et al. 2001, Awaki et al. 2000); 2) the observed spectral variation requires a change in  $N_{\rm H}$  of the neutral ( $\Delta N_{\rm H} \sim 5.5 \times 10^{22} {\rm cm}^{-2}$ ) and one of the ionised absorbers ( $\Delta N_{\rm H} \sim 6.7 \times 10^{22} {\rm cm}^{-2}$ ).
- We find the presence of the Fe K $\alpha$  emission line, with equivalent width  $EW\sim$ 81 eV during the Suzaku observation, in agreement with a fairly weak reflection contribution. During the XMM-Newton observation the equivalent width is lower ( $EW\sim$ 47 eV), and it could be responding to a past weaker continum, as was observed during earlier ASCA observations (Awaki et al.

- 2000). We do not observe any broadening of the Fe  $K\alpha$  line as expected for lines produced in the inner regions of the accretion disk, in agreement with the results of Smith et al. (2001) and Netzer, Turner, & George (1998).
- We detect a weak absorption line with an energy centroid at  $E \sim 7.4$  keV, consistent with a possible blueshifted 1s $\rightarrow$ 2p transition of FeXXVI (at 6.95 keV). We infer that the ionised absorber responsible for this feature has an observed outflow velocity of  $v_{out} \sim 0.05$  c. Higher resolution observations are needed in order to improve the significance of this detection.
- The long time elapsed between the two observations does not allow us to infer the time scale of the variability, so we can only determine upper limits on the distances of the ionised absorbers. However, as the mass of the central black hole is known from previous works, we can also estimate the minimum escape radius of the outflowing material. The ionisation parameters inferred for the two ionised absorbers suggest that one of them must be located at sub-parsec scales, and thus in the region ranging from the accretion disk to the BLR, while the second absorber is likely located at a parsec-scale distance.

#### ACKNOWLEDGMENTS

This research has made use of the NASA/IPAC Extragalactic Database (NED) which is operated by the Jet Propulsion Laboratory, California Institute of Technology, under contract with the National Aeronautics and Space Administration.

# REFERENCES

Antón S., Thean A., Browne I., Pedlar A., 2002, ASPC, 284, 289 Antonucci, R. 1993, ARA&A, 31, 473

Akylas, A., Georgantopoulos, I., Griffiths, R. G., Papadakis, I. E., Mastichiadis, A., Warwick, R. S., Nandra, K., & Smith, D. A. 2002, MNRAS, 332, L23

Arnaud, K. A. 1996, Astronomical Data Analysis Software and Systems V, 101, 17

Awaki H., Ueno S., Taniguchi Y., Weaver K. A., 2000, ApJ, 542, 175

Baird S.R., 1981, ApJ, 245, 208

Behar, E., Kaspi, S., Reeves, J., et al. 2010, ApJ, 712, 26

Bianchi, S., Guainazzi, M., Matt, G., et al. 2005, A&A, 442, 185 Bianchi, S., Guainazzi, M., & Chiaberge, M. 2006, A&A, 448, 499

Bianchi, S., Piconcelli, E., Chiaberge, M., et al. 2009, ApJ, 695, 781

Bianchi, S., Maiolino, R., & Risaliti, G. 2012, Advances in Astronomy, 2012,

Boldt, E. 1987, Phys. Rep., 146, 215

Braito V., Ballo L., Reeves J. N., Risaliti G., Ptak A., Turner T. J., 2013, MNRAS, 428, 2516

Dadina, M. 2008, A&A, 485, 417

de Vaucouleurs, G., de Vaucouleurs, A., Corwin, H., Buta, R. J., Paturel, G., & Fouqu, P. 1991, Third Reference Catalogue of Bright Galaxies (Berlin: Springer)

Done C., 2010, arXiv, arXiv:1008.2287

Elitzur M., 2008, NewAR, 52, 274

Elitzur M., 2012, ApJ, 747, L33

Elvis, M., Risaliti, G., Nicastro, F., Miller, J. M., Fiore, F., & Puccetti, S. 2004, ApJ, 615, L25

Elvis M., 2012, JPhCS, 372, 012032

Fukazawa Y., et al., 2009, PASJ, 61, 17

Ghisellini G., Haardt F., Matt G., 1994, MNRAS, 267, 743

Ghisellini, G., Haardt, F., & Matt, G. 2004, A&A, 413, 535

Gofford J., Reeves J. N., Tombesi F., Braito V., Turner T. J., Miller L., Cappi M., 2013, MNRAS, 430, 60

Gruber, D. E., Matteson, J. L., Peterson, L. E., & Jung, G. V. 1999, ApJ, 520, 124

Guainazzi M., Bianchi S., de La Calle Pérez I., Dovčiak M., Longinotti A. L., 2011, A&A, 531, A131

Horst H., Smette A., Gandhi P., Duschl W. J., 2006, A&A, 457, L17

Jansen, F., et al. 2001, A&A, 365, L1

Kaastra, J. S. & Mewe, R. 1993, A&AS, 97, 443

Kaastra, J. S., Mewe, R., Liedahl, D. A., Komossa, S., and Brinkman, A. C. 2000, A&A 354, L83

Kalberla P. M. W., Burton W. B., Hartmann D., Arnal E. M., Bajaja E., Morras R., Pöppel W. G. L., 2005, A&A, 440, 775

Kallman, T. R., Palmeri, P., Bautista, M. A., Mendoza, C., & Krolik, J. H. 2004, ApJS, 155, 675

Kaspi, S., Brandt, W. N., Netzer, H.et al. 2000a, ApJL 535, L17 Khachikian, E. Y., & Weedman, D. W. 1974, ApJ, 192, 581

Kokubun, M., et al. 2007, PASJ, 59, 53

Koyama, K., et al. 2007, PASJ, 59, 23

Kriss, G. A., Canizares, C. R., & Ricker, G. R. 1980, ApJ, 242, 492

Laor A., 1991, ApJ, 376, 90

Lutz D., Maiolino R., Spoon H. W. W., Moorwood A. F. M., 2004, A&A, 418, 465

Maiolino, R., Risaliti, G., Salvati, M., et al. 2010, A&A, 517, A47 Magdziarz, P., & Zdziarski, A. A. 1995, MNRAS, 273, 837

Marchese E., Braito V., Della Ceca R., Caccianiga A., Severgnini P., 2012, MNRAS, 421, 1803

Markowitz A., Krumpe M., Nikutta R., 2013, HEAD, 13, #108.10 Matt G., Brandt W. N., Fabian A. C., 1996, MNRAS, 280, 823

Mewe, R., Gronenschild, E. H. B. M., & van den Oord, G. H. J. 1985, A&AS, 62, 197

Miller, J. S. & Goodrich, R. W. 1990, ApJ, 355, 456

Mitsuda, K., et al. 2007, PASJ, 59, 1

Murphy K. D., Yaqoob T., 2009, MNRAS, 397, 1549

Nandra K., O'Neill P. M., George I. M., Reeves J. N., 2007, MN-RAS, 382, 194

Netzer H., Turner T. J., George I. M., 1998, ApJ, 504, 680

Neff S. G., de Bruyn A. G., 1984, IAUS, 110, 263

Nenkova M., Sirocky M. M., Nikutta R., Ivezić Ż., Elitzur M., 2008, ApJ, 685, 160

Nenkova M., Sirocky M. M., Ivezić Ž., Elitzur M., 2008, ApJ, 685, 147

Nikolajuk M., Papadakis I. E., Czerny B., 2004, MNRAS, 350, L26

Palmeri, P., Mendoza, C., Kallman, T. R., Bautista, M. A., & Meléndez, M. 2003, A&A, 410, 359

Puccetti, S., Fiore, F., Risaliti, G., et al. 2007, MNRAS, 377, 607 Risaliti, G. 2002, A&A, 386, 379

Risaliti, G., Elvis, M., & Nicastro, F. 2002, ApJ, 571, 234

Risaliti, G., Bianchi, S., Matt, G., Baldi, A., Elvis, M., Fabbiano, G., & Zezas, A. 2005, ApJ, 630, L129

Risaliti, G., Elvis, M., Fabbiano, G., et al. 2007, ApJ, 659, L111 Risaliti, G., et al. 2009, MNRAS, 393, L1

Risaliti, G., Elvis, M., Bianchi, S., & Matt, G. 2010, MNRAS, 406, L20

Risaliti, G. 2010, in American Institute of Physics Conference Se-

- ries, Vol. 1248, American Institute of Physics Conference Series, ed. A. Comastri, L. Angelini, & M. Cappi, 351?354
- Rivers E., Markowitz A., Rothschild R., 2011, ApJ, 742, L29
- Rivers E., Markowitz A., Rothschild R., 2013, ApJ, 772, 114
- Simpson C., Mulchaey J. S., Wilson A. S., Ward M. J., Alonso-Herrero A., 1996, ApJ, 457, L19
- Singh V., Shastri P., Risaliti G., 2011, A&A, 532, A84
- Smith, D. A., Georgantopoulos , I., Warwick, R. S., 2001, ApJ, 550, 635
- Strüder, L., et al. 2001, A&A, 365, L5
- Takahashi, T., et al. 2007, PASJ, 59, 35
- Tombesi F., Cappi M., Reeves J. N., Palumbo G. G. C., Yaqoob T., Braito V., Dadina M., 2010, A&A, 521, 57
- Tombesi F., Cappi M., Reeves J. N., Palumbo G. G. C., Braito V., Dadina M., 2011, ApJ accepted
- Tombesi F., Cappi M., Reeves J. N., Nemmen R. S., Braito V., Gaspari M., Reynolds C. S., 2012, arXiv, arXiv:1212.4851
- Tombesi F., Cappi M., Reeves J. N., Nemmen R. S., Braito V., Gaspari M., Reynolds C. S., 2013, MNRAS, 430, 1102
- Turner T. J., Perola G. C., Fiore F., Matt G., George I. M., Piro L., Bassani L., 2000, ApJ, 531, 245
- Turner, M., et al. 2001, A&A, 365, L27
- Turner T.J., Miller L., 2009, A&ARv, 17, 47 5
- Turner, T. J., Miller, L., Kraemer, S. B., Reeves, J. N., & Pounds, K. A. 2009, ApJ, 698, 99
- Turner, T. J., Miller, L., & Tatum, M. 2012, American Institute of Physics Conference Series, 1427, 165
- Unger S. W., Pedlar A., Neff S. G., de Bruyn A. G., 1984, MN-RAS, 209, 15P
- Urry, C. M., & Padovani, P. 1995, PASP, 107, 803
- Warwick, R. S., Koyama, K., Inoue, H., Takano, S., Awaki, H., & Hoshi, R. 1989, PASJ, 41, 739
- Wilms J., Allen A., McCray R., 2000, ApJ, 542, 914
- Woo J.-H., Urry C. M., 2002, ApJ, 579, 530
- Xue S.-J., Otani C., Mihara T., Cappi M., Matsuoka M., 1998, PASJ, 50, 519